Multi-source multi-receiver microseismic reflection imaging: case study Basel

A. Reshetnikov, J. Kummerow, S. A. Shapiro, FU Berlin, H. Asanuma, Tohoku University and M. Häring, Geothermal Explorers International Ltd.*

SUMMARY

In this paper Microseismic Reflection Imaging (MRI) approach is applied to the high quality microseismic data from the stimulation of Enhanced Geothermal System (EGS) at Basel. Microseismic waveforms recorded at a number of downhole stations are analysed and the presence of reflections is revealed. The MRI approach is applied to the data recorded at two different borehole instruments: 2.5 km and 4.3 km away from the injection interval. The results complement each other and represent the detailed high resolution fracture map of the reservoir in the vicinity of the microseismic cloud. In addition to the standard sections of the images, the 3D structure of the first order cracks is shown. A possible joint interpretation of the obtained images and the event location is presented.

INTRODUCTION

The geothermal project in Basel, Switzerland, was started in 2006 with the aim to build a plant producing both electricity and heat directly in the urban area. A real-time microseismic monitoring network containing a number of shallow and deep borehole sensors was installed. The stimulation well Basel 1 was drilled to the total depth of 5 km (Häring et al. (2008)). In order to enhance the permeability of the granitic basement, Basel 1 well was stimulated with the total amount of 11,570 m^3 of water. After 6 days of stimulation (2–8 December 2006), it was stopped due to unexpectedly high microseismic activity with event magnitudes up to M_L 2.6. However, activity remained significant and decreased slowly. Up to the end of November 2007, multiple events were recorded with maximal magnitude M_L 3.4 (Häring et al. (2008)). Later the independent seismic hazard risk analysis was performed which followed by the local authorities decision to completely stop the project (Bachmann et al. (2011)). Nevertheless the microseismic events recorded at Basel microseismic monitoring system represent a great possibility for further understanding of the physics of induced seismicity.

MICROSEISMIC MONITORING SYSTEM

The microseismic waveforms during and after reservoir stimulation were recorded by several networks operated by independent institutions (the list can be found in Deichmann and Ernst (2009)). In this study, the network operated by Geothermal Explorers Ltd. was considered. This network includes six three-component downhole sensors in long-term operation (Figure 1). There are five shallow stations in sediments layer: STJ, MAT, HAL, OT1 and RI2. There is also one deeper geophone OT2 located in Crystalline basement at 2740 m depth and 2 km SE from the treatment borehole.

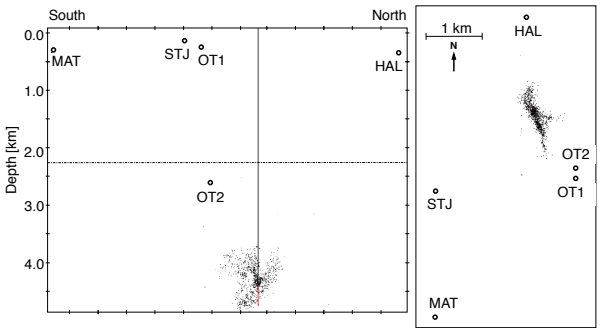

Figure 1: Distribution of downhole sensors. Left: side view. Right: map view. Black dots – distribution of the located microseismic events, black solid line – treatment borehole, red solid line – open hole section.

MICROSEISMIC WAVEFORMS

The first induced microseismic event was detected nearly 4 hours after the start of the Basel 1 borehole stimulation. In total, during six days of the stimulation 11,200 events were detected. After stopping the injection, seismic activity remained high, and until the end of November 2007 about 3700 more events were recorded (Häring et al. (2008)). In this study, 3068 events from both injection and post-injection phases were analysed.

An example of the unprocessed microseismic waveforms recorded at two sensors used for imaging is presented in Figure 2. This event was recorded on 08 Dec 2006, 01h 30m and represents the common signal quality among the analysed data. All the downhole sensors recorded three component traces.

Due to the different distances between sensors and injection interval, the frequency content and the amplitude ranges differ for different 3C traces. Nevertheless, the quality of the data allows one to easily identify direct P- and S- arrivals for all six recordings. There are also some relatively strong phases which are not associated with the direct waves. This can be an indirect indication of reflections which means the presence of reflective objects in the vicinity of this event or receiver.

MICROSEISMIC EVENT DISTRIBUTION

The location procedure used in further considerations was performed by the method of Kummerow et al. (2011) and further improved by Kummerow et al. (2012). In total 2456 microseismic events were located including 1117 multiple events (see Figure 3). The size of the maximal cluster is around 200 events. The seismically active volume extends about 1000 m in the direction of the main horizontal trend, around 400 m in WE direction and 1000 m in vertical direction.

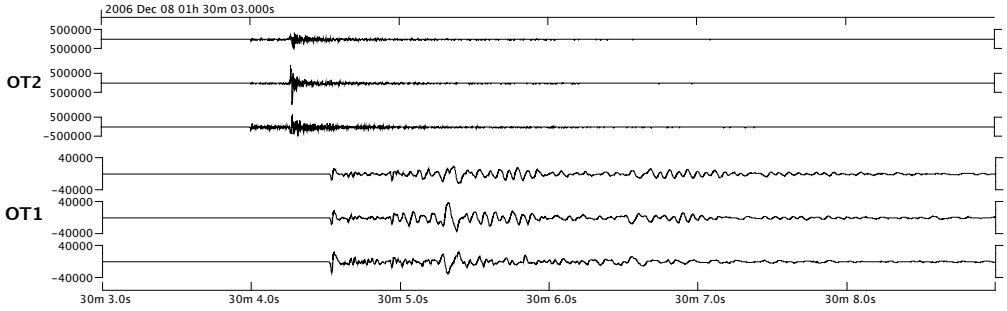

Figure 2: An example of an event recorded by two borehole sensors. The recording time is 08 Dec 2006, 01h 30m, trace length is 6 seconds. Stations are sorted according to the distance from the injection interval. Amplitude units are micro volts [μV].

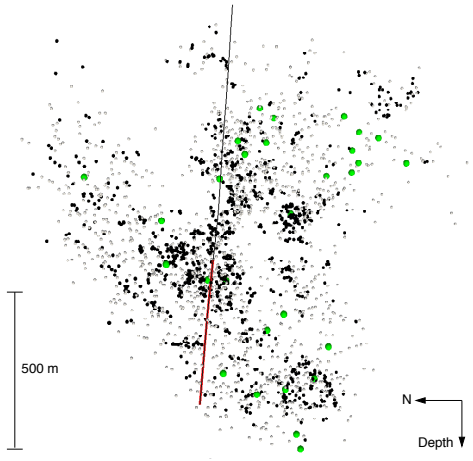

Figure 3: Location of 2138 microseismic events. Black solid curve – borehole, red solid curve – open hole section, green spheres – big events, black dots – clustered events, gray dots – non-clustered events.

The distribution of the located events shows nearly vertical structures. In map view, the cloud splits up into two pronounced planar structures. The major one has an azimuth of $N153 \pm 5^{\circ}E$ which is close to SHmax direction estimated from induced tensile fractures as $N151 \pm 13^{\circ}E$ (Dyer et al. (2008)). The second branch, started close to the well treatment interval and prolongated in the eastern direction and has an azimuth of $N100 \pm 5^{\circ}E$.

There are also less pronounced but noticeable features in the vertical section along the direction of the main cloud. This is a number of steeply dipping structures at both sides of the treatment interval with dips about 60°, which is consistent with the dominant dips of natural fractures detected at this interval of the treatment borehole (Häring et al. (2008)).

MICROSEISMIC REFLECTION IMAGING APPROACH

The idea of Microseismic Reflection Imaging is to treat a located microseismic event as a standard active seismic source and to use the corresponding recorded wavefield as a reflection seismic shot gather for VSP or a single recording for a single geophone (Reshetnikov et al., 2010). Reflections within the seismograms can be then imaged by using migration techniques adapted from reflection seismics.

Usually, the number of microseismic events is much larger than the number of seismic sensors. The distances between receivers can be significant which implies a necessity to process the traces recorded at different stations independently. In order to facilitate the seismic data pre-processing and to present it in a more common way, sources and receivers can be swapped. Then the system of the microseismic cloud and the acquisition can be considered as several “sources” and the cloud of spatially distributed “receivers”.

The seismic data recorded at a geophone is a continuous three component data stream which is supplemented by preliminary picked P- and S- arrival times for different microseismic events. Assuming that the hypocenter locations and origin times are determined, one can extract the 3C traces for each event and shift it to its origin time. Then these traces can be sorted according to the distance from the geophone to the event and merged into the seismic gather. Such gather is not a complete analogue of VSP seismic gather, but since the events are located within relatively dense cloud with roughly similar inter-event distance, one can clearly see the direct P- and S- arrivals and possible presence of the reflections.

For Basel data the spatial dimensions of a microseismic cloud are small in regard to the distances from the events to the receivers (see Figure 1). Accordingly, the aperture of scattered waves for such system is extremely low in comparison to a wide-angle active seismic profiling data. In this situation the only way to get a reliable image is to take into account the polarity of the reflected waves.

In order to construct an image the Fresnel-Volume-Migration method (Lüth et al., 2005; Buske et al., 2006) was applied. This is an extension of the pre-stack Kirchhoff depth migration which uses the wavefield polarization information to restrict the migration operator to a region around the actual reflection point. The procedure itself resolves spatial ambiguities caused by, for instance, limited aperture and results in strongly reduced migration artefacts, particularly for data sets with low

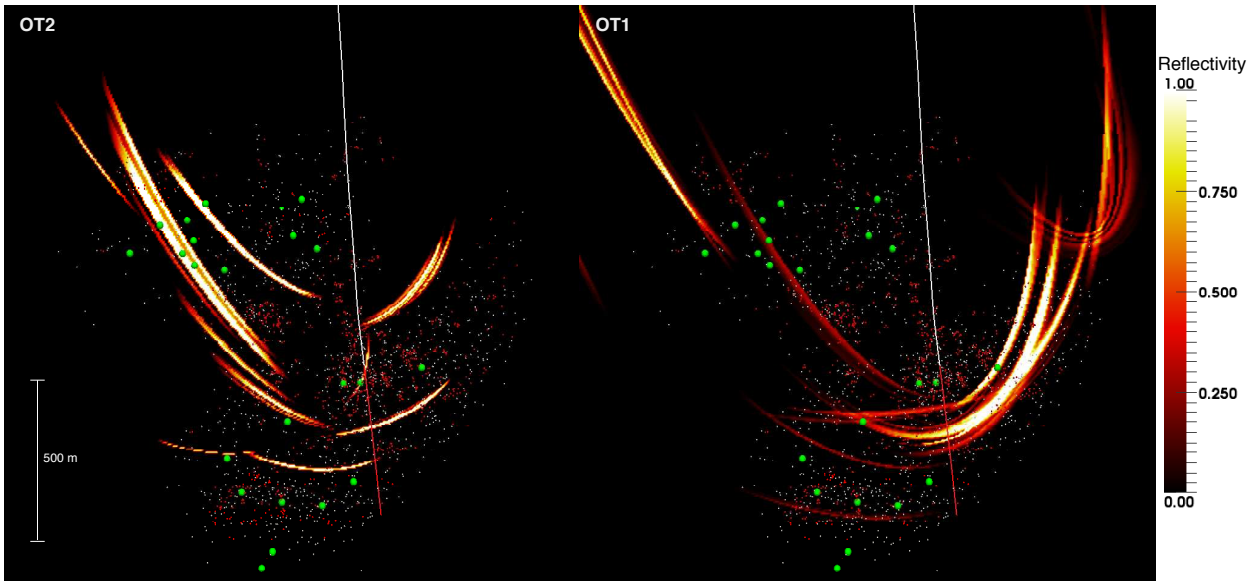

Figure 4: Vertical sections of the obtained images for OT2 (left) and OT1 (right) stations. White solid line – borehole, red dots – clustered events, white dots – non clustered events, green dots - big events, red solid line – borehole open hole section.

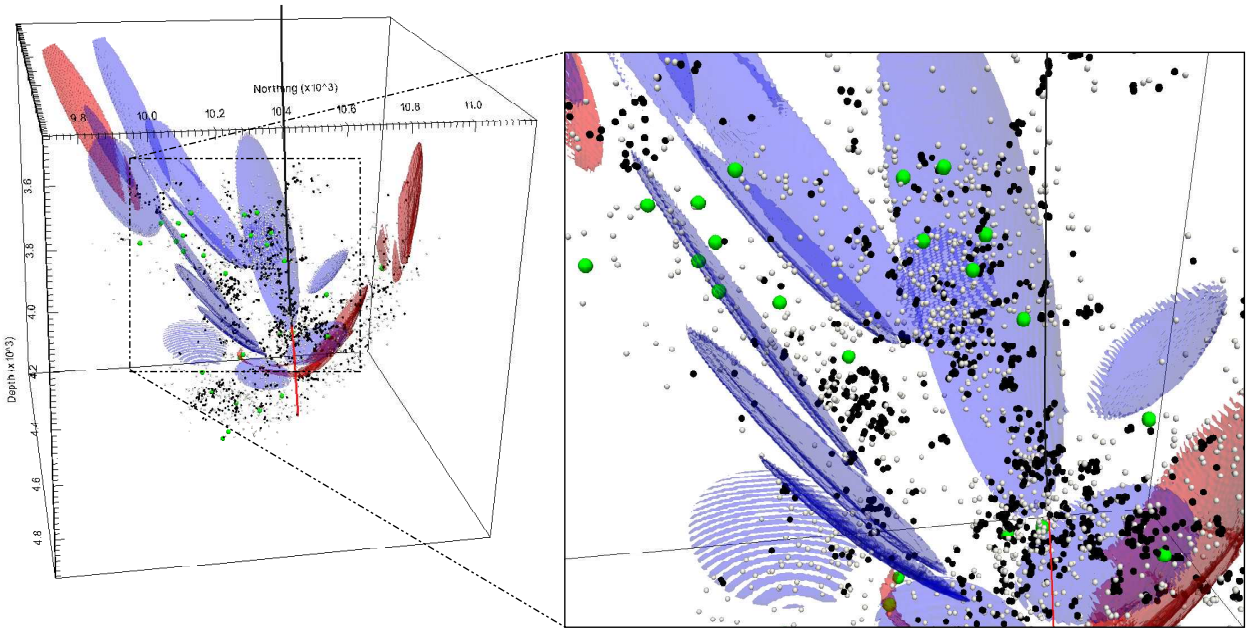

Figure 5: 3D Iso-surfaces corresponding to the highest reflective areas in both images (blue – OT2 image, red – OT1 image). Left: complete migration cube view. Right: zoomed central part of the image.

coverage.

To obtain the polarization of the wavefield, we use auto- and cross-variances of time samples within a time window, including several dominant periods of the P- or S-wave (Jurkevics, 1988).

IMAGING RESULTS

In this study the data recorded at OT2 and OT1 stations were used (see Figure 1). OT2 station located 1.1km SE from injection well at 2487 m depth was chosen as the closest station to the cloud (except of BS1 station which malfunctioned after several hours of the injection). The second station OT1 located at 247 m depth, 2 km above OT2. For imaging, events with the best signal to noise ratio and the smallest location residuals were selected. In total, 600 events for OT2 and 400 events for OT1 were used.

Here we present the image of the wavefield between direct P- and S- waves which we interpreted as PP reflections. In Figure 4 one can see the vertical sections along the main trend of the cloud for both obtained images in the vicinity of the open hole section. In Figure 5 the 3D iso-surfaces corresponding to the strongest reflectivity areas for both images are presented. The results complement each other and demonstrate the same structure of reflectors within the stimulated reservoir. The overall shape of the reflectors correlates with the shape of the microseismic cloud. There are some groups of the events which are not associated with any reflector in the image. This can be explained by the geometry of the acquisition system. The features corresponding to these groups of events cannot be illuminated by other events. The strongest reflectors in the image are confirmed by the information about cracks in the borehole. In Häring et al. (2008) it is noted that the bottom part of the well including the open hole is characterised by natural fracture sets trending NW-SW to NNW-SSE, with steep dips exceeding 60°. Among the inclined fractures there are also several sub-horizontal reflectors within the open hole section in the image.

DISCUSSION

In order to produce visible reflections, which can be migrated by the imaging procedure, a reflector must have a significant contrast of physical properties in comparison with the background medium. Therefore, the second order cracks produced by simple slip can be unlikely seen in the image. Figure 6 shows a sketch representing a possible interpretation of the microseismic event locations and the obtained reflectors. Reflectors in the image probably are cracks with a higher permeability compared to the background rock. These first order fractures serve as pathways for the fluid and the elevated pressure to the medium and therefore control the shape of the cloud which is confirmed by the observation. The majority of microseismicity occurs not in these pathways but in the surrounding rock. Clustered events could occur in the second order cracks branching from the main pathways. Waveform similarity of events in the clusters can be explained by the fact that they occur at the same or at parallel systems of the second-order fractures. Non-clustered events are either two small to be identified as a part of a cluster or have a specific source mechanism. Possibly, these events can occur as a result of pore pressure perturbation in the background rock.

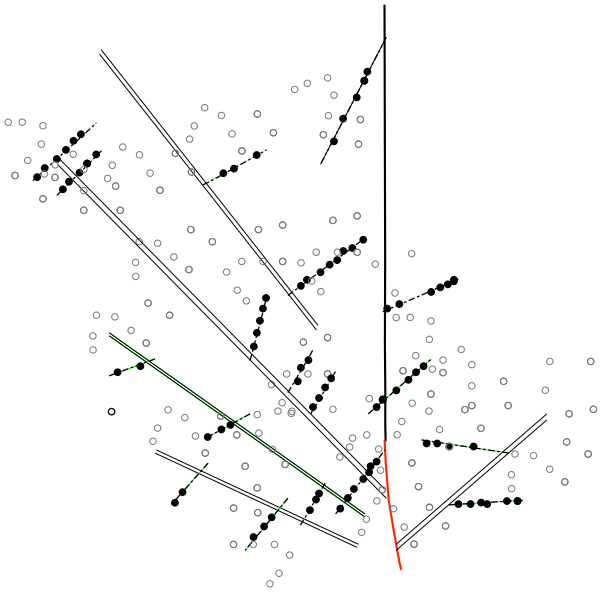

Figure 6: Possible interpretation of the induced microseismicity. Black and red curves – borehole geometry and open hole section. Black solid lines – first order cracks, dashed lines – second order cracks. Black dots – clustered events, gray circles – non clustered events.

CONCLUSIONS

The Microseismic Reflection Imaging approach was applied to the Basel 1 data recorded at two different borehole instruments, 2.5 km and 4.3 km away from the injection interval. Both imaging results complement each other and show the same structure of reflectors within the stimulated reservoir. The overall shape of the reflectors correlates with the shape of the microseismic cloud. A possible joint interpretation of the obtained and the microseismic event locations images is presented.

ACKNOWLEDGMENTS

We thank the sponsors of the *PHASE consortium* for supporting the research presented in this paper.

REFERENCES

Bachmann, C. E., S. Wiemer, J. Woessner, and S. Hainzl, 2011, Statistical analysis of the induced Basel 2006 earthquake sequence: introducing a probability-based monitoring approach for Enhanced Geothermal Systems: Geophysical Journal International.

Buske, S., M. Heigel, and S. Lüth, 2006, Fresnel-volume-migration of single-component seismic data: EAGE 68th annual meeting and technical exhibition, Vienna, Expanded Abstracts, **G044**.

Deichmann, N., and J. Ernst, 2009, Earthquake focal mechanisms of the induced seismicity in 2006 and 2007 below Basel (Switzerland): Swiss Journal of Geosciences, **102**, no. 3, 457–466. (10.1007/s00015-009-1336-y).

Dyer, B. C., U. Schanz, F. Ladner, M. O. Häring, and T. Spillman, 2008, Microseismic imaging of a geothermal reservoir stimulation: The Leading Edge, **27**, 856–869.

Häring, M., U. Schanz, F. Ladner, and B. Dyer, 2008, Characterisation of the Basel 1 enhanced geothermal system: Geothermics, **37**, 469–495.

Jurkevics, A., 1988, Polarization analysis of three-component array data: Bulletin of the Seismological Society of America, **78**, 1725–1743.

Kummerow, J., A. Reshetnikov, M. Häring, and H. Asanuma, 2012, Distribution of the Vp/Vs Ratio within the Basel 1 Geothermal Reservoir from Microseismic Data: Expanded abstracts, EAGE 74th annual meeting and technical exhibition, Copenhagen.

Kummerow, J., S. Shapiro, H. Asanuma, and M. Häring, 2011, Application of an Arrival Time and Cross Correlation Value-based Location Algorithm to the Basel 1 microseismic Data: Expanded abstracts, EAGE 73th annual meeting and technical exhibition, Vienna.

Lüth, S., S. Buske, A. Görtz, and R. Giese, 2005, Fresnel-volume-migration of multicomponent data: Geophysics, **70**, S121–S129.

Reshetnikov, A., S. Buske, and S. A. Shapiro, 2010, Seismic imaging using microseismic events: Results from the San Andreas Fault system at SAFOD: J. Geophys. Res., **115**, B12324.